Indian Journal of Chemical Technology
Vol. 32, May 2025, pp. 324-333
DOI: 10.56042/ijct.v32i3.15371

Multifaceted material characterization and biocompatibility evaluation of polylactic acid nanocomposites reinforced with palmyra nanofibrillated cellulose

S A Priya* & N T Nevaditha

Department of Chemistry & Research, Nesamony Memorial Christian College, Marthandam -629165, Tamil Nadu, India

*E-mail: sathyarajsathya1961@gmail.com

Received 30 November 2024; accepted 19 March 2025

Eco-conscious nanocomposites are developed by embedding nanofillers into biopolymeric matrices, enhancing their properties in various aspects. Polylactic acid (PLA), a naturally degradable thermoplastic derived from renewable resources, is renowned for its sustainable and eco-friendly attributes. However, despite extensive research on PLA-based nanocomposite films, there is a gap in studies exploring PLA reinforced with Palmyra nanofibrillated cellulose (NFC). This study explores the incorporation of Palmyra NFC into PLA using the solution casting method to improve its thermal, mechanical, bactericidal, and biosafety properties. FTIR analysis reveals the formation of hydrogen bonds between the hydroxyl (–OH) moieties of NFC and the carbonyl (C=O) in PLA, which helps the compatibility and dispersion of the components. Thermal analysis shows 27°C increase in thermal degradation temperature compared to plain PLA. The addition of NFC increases the tensile strength and modulus of PLA nanocomposites by 68.8% and 89.4%, respectively. The antibacterial performance improves with higher NFC content, inhibiting bacterial growth more effectively than plain PLA. The hemolysis and MTT assays demonstrate good red blood cell compatibility and high cell viability, confirming the excellent biocompatibility of the 3 wt% NFC reinforced PLA nanocomposite at below 200 µg/mL concentrations. The improvements in thermal stability, mechanical strength, antibacterial properties, and biocompatibility suggest that these nanocomposites can meet the demanding requirements of biomedical materials.

Keywords: Antibacterial, Biocompatibility, Nanocomposites, Palmyra Fibers, Polylactic acid

Introduction

Polylactic acid (PLA) is a biobased polymer synthesized through either ring-opening polymerization or polycondensation of lactic acid. Its lactide monomer is sourced from the fermentation of various carbohydrate rich sources such as corn, sugarcane, and wheat[1,2]. Its inherent properties of biocompatibility, reusability, composability, and renewability have enabled substantial advancements in numerous applications, especially in the fields of packaging and biomedicine[3,4]. On the contrary, it also carries some drawbacks, which includes hydrophobicity, poor heat stability, brittleness and a high price point. The enhancement of PLA properties is vital for ensuring its competitiveness in relation to other plastic materials[5-7]. Bio-based nanocomposites have become increasingly popular because of their organic breakdown capacity, biological acceptance, and good processability when compared to plain polymers[8-10]. These types of composites have extensive applications in the field of food packaging, biomedical and tissue engineering with improved thermal and mechanical properties[11,12].

There has been significant increase in attention toward nanofibrillated cellulose, emphasizing their potential as a viable alternative for micro-sized reinforcements in composite materials. Moreover, numerous research efforts have been undertaken to investigate the efficacy of nanofibrillated cellulose (NFC) as reinforcements within various polymer matrices, such as PVA, natural rubber, and polylactic acid[13]. NFC are emerging as a promising and economical nanomaterial that can enhance the structural integrity of nanocomposites through reinforcement[14,15]. The main reasons for the use of cellulosic materials are their good mechanical properties, fully degradable and renewable character, which set them apart from inorganic fillers[16]. Thus, the incorporation of nano-sized natural fibers into PLA matrix constitutes a promising strategy for enhancing its performance. The most commonly used bio-based materials by researchers in the production of PLA-based nanocomposites are largely sourced from agricultural byproducts and fibers of sugarcane bagasse, cotton, ramie, hemp, sisal, and flax[17]. The incorporation of NFC to biopolymer yields numerous

benefits, such as high surface area increased stiffness, enhanced crystallinity, biodegradability, and additional specific properties, all achieved with minimal input levels. The nanoscale dimensions and favourable properties of NFC encourage the exploitation of agricultural waste as a key source of cellulose[18].

As far as we know, this is the first report on the reinforcement of nanocomposite films with unmodified NFC derived from palymra leaves. The palmyra tree, or *Borassus flabellifer*, is a member of the Arecaceae family, capable of growing up to 30 meters tall, adorned with bluish-green canopy leaves. These leaves are used producing of various indigenous products such as mats, baskets, brooms, ropes, and fans. The fruit pulp is traditionally used in culinary practices, while the sap is recognized as a sweetener suitable for those with diabetes[19,20]. This study investigates the potential use of NFC obtained from palmyra leaves by chemical and mechanical treatments, as reinforcing agents for PLA nanocomposites which could bring new properties to the material. These nanocomposites were characterized in terms of crystallinity, thermal behaviour, surface morphology, chemical interactions, and mechanical properties. Antibacterial activity and biocompatibility were also assessed to evaluate their potential for biomedical applications.

Experimental section

Materials

Matured leaves of the palmyra tree were collected from local areas in Marthandam, India. Poly (lactic acid) (PLA) (Luminy 175) in granule form, used as the polymer matrix, was purchased from 2M Biotech LLP, NatureWorks (India). Dichloromethane and sodium hydroxide were obtained from Spectrochem (Mumbai), while glacial acetic acid and sodium chlorite were purchased from Molychem (India). Ethylene glycol dimethylacrylate (EDGMA) was received from Sigma-Aldrich. All chemicals were of analytical grade and used as received. Castor oil (Poorna brand) was purchased from a supermarket. Distilled water was used in this study for the preparation of nanofibrillated cellulose (NFC).

Extraction and purification of NFC

Nanofibrillated cellulose (NFC) were extracted from Palmyra leaves through series of procedures. The leaves were cut into 1 cm pieces, washed with distilled water to remove impurities, and left to dry in the sun, becoming crisp and brittle. After drying, the leaves were ground and sieved to obtain a fine greenish powder, which served as the starting material for the chemical treatments to extract the cellulose. The ground material was then treated with a 4% sodium hydroxide (NaOH) solution and heated at 80°C for 1 h to remove hemicellulose, lignin, and other impurities and leave behind purer cellulose. The fibers were washed with distilled water until the pH became neutral. Next, the fibers were bleached by boiling in a mixture of 1.5 g sodium chlorite and 1.5 g acetic acid at 80°C for 3 h to further refine the cellulose. Finally, the fibers were rinsed and oven-dried at room temperature until constant weight was achieved.

Film fabrication

The PLA polymeric solution was prepared by dissolving PLA granules in dichloromethane with continuous stirring until the granules were fully dissolved. EGDMA was added as a crosslinking agent, and 10% castor oil was incorporated as a plasticizer. The mixture was stirred until a homogeneous solution was obtained. The resulting solution was then poured onto a clear glass mold and allowed to dry for 24 h. The formed films, measuring approximately 10 × 10 cm, were labeled as plain PLA. For the PLA nanocomposite films, NFC was added in varying concentrations (1 to 5 phr) to the PLA solution, and the mixtures were stirred to ensure uniform dispersion. The solutions were then cast onto glass plates using the same drying method. The nanocomposite films were designated as PLPF1, PLPF2, PLPF3, PLPF4, and PLPF5 based on their respective NFC content.

Characterization studies

FTIR spectra were obtained using Thermo Fisher spectrometer equipped with a UATR accessory, covering the range of 4000–500 cm^{-1} with resolution of 4 cm^{-1}. XRD analysis was performed using a Bruker D8 Advance diffractometer with Cu-Kα radiation, operated at 30 mA and 40 kV, recording data between 10° and 50° at a scanning speed of 4°/min. The surface morphology of NFC and nanocomposites was examined using JEOL JSM-IT200 SEM at an acceleration voltage of 10 kV after gold sputter-coating. Thermal stability was evaluated using a Shimadzu DTG 60H TGA by heating the samples from 100°C to 800°C under nitrogen flow of 20 mL/min.

Tensile strength test

Mechanical testing was done using the Instron 3345 Universal Tester equipped with 500N load cell to measure the tensile strength at the point of breakage for each sample. In accordance with ASTM D882, the films were cut into strips measuring 75 mm x 10 mm. A fixed crosshead speed of 10 mm/min and a gauge length of 30 mm were employed in all tests. Three specimens from each composition were tested, and the average values were calculated.

Antibacterial activity

Antibacterial study was conducted on the PLA and PLA nanocomposite films against two Gram-positive bacteria *Bacillus subtilis* and *Staphylococcus aureus* and two Gram-negative bacteria *Escherichia coli* and *Pseudomonas aeruginosa* using Kirby-Bauer test. A bacterial suspension is prepared and standardized to match a 0.5 McFarland turbidity standard. Using a sterile swab, the bacterial suspension is spread evenly across the agar plate. The test samples discs are then placed on the agar surface using sterile forceps. The plates are incubated at 35–37°C for 16–18 h, after which the zones of inhibition around each disc are measured.

Hemolytic assay

Human blood (5 mL) was collected from healthy volunteers with 3.8% sodium citrate as an anticoagulant. The blood was washed three times with 0.9% NaCl saline, then centrifuged at 1500 rpm for 5 min to separate plasma and the white buffy layer. The erythrocytes were washed three times with 1X phosphate buffer saline (PBS) at pH 7.4 and suspended in a 1:9 ratio with phosphate buffer saline. The erythrocyte suspension was incubated with different concentrations of the test sample (PLPF3), 1X PBS (negative control), and 1% Sodium dodecyl sulfate (positive control) at 37°C for 60 min. After centrifugation, the hemoglobin concentration in the supernatant was measured at 540 nm using spectrophotometer. The hemolysis percentage was calculated based on absorbance compared to the positive control. The formula for calculating the percentage of hemolysis is as follows:

$$\text{Hemolysis (\%)} = (\text{Test OD}/\text{Control OD}) \text{ X } 100 - \text{Negative control}$$

MTT assay

The MTT assay (3-(4,5-Dimethylthiazol-2-yl)-2,5-diphenyltetrazolium bromide Assay) is a colorimetric test for measuring the activity of enzymes that reduce 3-(4,5- dimethylthiazol-2-yl)-2,5 diphenyltetrazolium bromide, (MTT) to formazan, giving a purple colour. The in vitro cytotoxicity of PLPF3 was assessed using the MTT assay with peripheral blood mononuclear cells (PBMCs). The cells were cultured in Dulbecco's Modified Eagle Medium (DMEM) supplemented with 10% Fetal Bovine Serum (FBS) and antibiotics in a 96-well plate and incubated at 37°C in a 5% CO_2 atmosphere for 24-48 h. After washing with PBS (Phosphate-Buffered Saline), the cells were treated with various concentrations of PLPF3 in serum-free DMEM for 24 h. Following this, MTT reagent was added and incubated for 2–4 h, allowing the formation of purple formazan crystals. After incubation, the crystals were dissolved in DMSO, and absorbance at 570 nm was measured. The absorbance values are then compared between the test sample, positive control, and negative control to calculate the percentage of cell viability.

$$\text{Cell viability \%} = (\text{Test OD}/\text{Control OD}) \text{ X } 100$$

Results and Discussion

Infrared spectral analysis

The spectra for NFC shown in Fig. 1 exhibit a broad peak at 3402 cm^{-1}, attributed to the –OH stretching vibrations of hydroxyl groups, indicating their abundance. The peak at 1249 cm^{-1} represents the C-O-H stretching vibration. Furthermore, absorption peaks at 1033 cm^{-1} and 894 cm^{-1} are attributed to C-O stretching and C^1-H bending vibration of cellulose. The peak at 1165 cm^{-1} linked to symmetric C–O–C stretching vibrations of cellulose chain. In PLA the peaks appear at

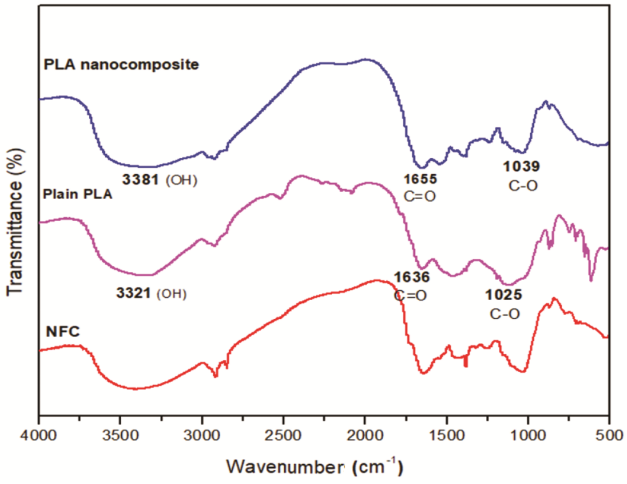

Fig. 1 — Infrared spectra of NFC, plain PLA and PLA nanocomposite

2925 cm^{-1} and 2851 cm^{-1}, corresponding to CH asymmetric and symmetric stretching vibrations of $–CH_2$ and $–CH_3$ groups in PLA. The strong absorption band at 1636 cm^{-1} indicates the presence of the C=O group, while peaks at 1410 cm^{-1} and 1340 cm^{-1} are assigned to $–CH_2$ bending and C–OH bending vibrations, respectively. The peak at 1181 cm^{-1} is related to the C-O stretching vibration of PLA of ester linkage[21,22]. The FTIR spectra of the PLA nanocomposite shows several changes in peak intensity and position can be observed compared to plain PLA. The broad peak observed around 3381 cm^{-1} becomes more pronounced in the nanocomposite, indicating stronger hydrogen bonding between the –OH groups of NFC and the C=O groups in PLA. The strong 1636 cm^{-1} peak, associate with C=O stretching in PLA, shows slight shifts in the nanocomposite, reflecting interactions with NFC. The 1254 cm^{-1} peak, specific to C–O stretching in cellulose, confirms the incorporation of NFC in the nanocomposite. Additionally, slight shifts and moderate intensity changes in the 1000–1200 cm^{-1} region, associated with C–O and C–O–C stretching, indicate molecular-level interactions between PLA and NFC. These changes collectively suggest improved dispersion and interfacial bonding within the PLA matrix, contributing to the enhanced properties of the nanocomposite [23].

Crystallographic analysis

The XRD analysis reveals the crystallographic characteristics and phase interactions of NFC, plain PLA and PLA nanocomposites (Fig. 2). The XRD pattern of NFC shows characteristic peak at around 2θ at 15.3°, 22.3°and 34.8° which are typical of the cellulose I crystalline structure. These peaks reflect the highly ordered, crystalline nature of NFC. The particle size of the NFC estimated to be about 61 nm using the Scherrer equation indicates nanoscale structure. The percentage of crystallinity and crystallinity index in plain PLA and PLA nanocomposites are given in Table 1. This small size contributes to large surface area and a 65% crystallinity index, which points out the superior mechanical properties of NFC and their ability to enhance the reinforcing capabilities in nanocomposites because of the high crystallinity index of reinforcing agent for PLA [24, 25]. The X-ray diffractogram of PLA show peaks at 2θ = 16.6° and 19.2° reflecting its semi-crystalline nature. The peak at 22.3° in the nanocomposites corresponds to the preserved crystalline structure of NFC, and the shift to 22.7° suggests phase interactions between PLA and NFC, indicating

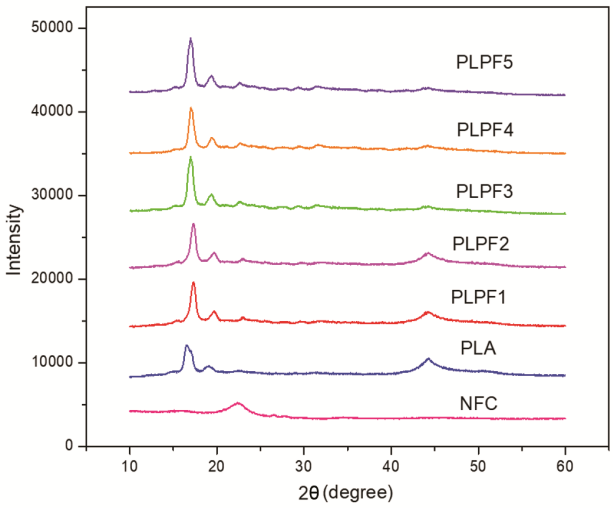

Fig. 2 — XRD pattern of NFC, plain PLA and PLA nanocomposites

Table 1 — Evaluation of crystallinity in plain PLA and PLA nanocomposites

Samples	Percentage of crystallinity	Crystallinity index
PLA	75.2	65.5
PLPF1	77.1	68.4
PLPF2	80.6	71.2
PLPF3	81.5	72.3
PLPF4	82.8	73.2
PLPF5	84.7	74.1

successful integration of NFC into the PLA matrix. The PLA nanocomposites also exhibit sharper and more pronounced peaks of 16.6°, 19.2°, 22.3° indicating an increase in crystallinity compared to plain PLA. This is due to the nucleating effect of NFC, which promotes PLA crystallization. However, variations in peak intensity and shape suggest that the degree of crystallinity and phase interactions depends on NFC loading.

Morphological studies

The surface morphologies of NFC, plain PLA and PLA nanocomposites are presented in Fig. 3(a)-3(d). The NFC in Fig. 3(a) appear as fine, elongated strands arranged in parallel fashion. The Fig. 3(b) depicts surface of plain PLA is smooth and uninterrupted, which indicates homogeneity without considerable structural variation. The PLA nanocomposite with 2 wt% NFC (Fig. 3(c)) displays NFC are evenly spread throughout the polymer matrix which can improve interfacial bonding between the NFC and PLA. In addition, small pores are observed, likely due to the dispersion of NFC and evaporation of the solvent during the drying process[27,28]. However, at

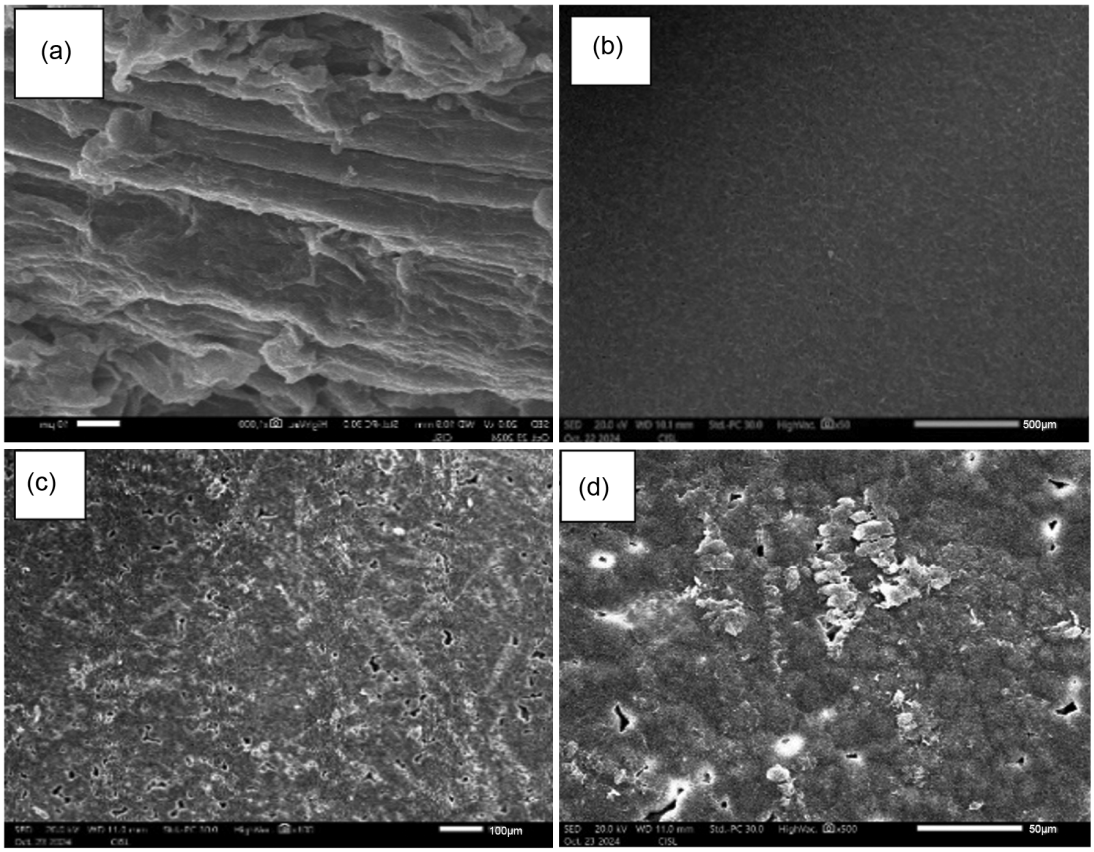

Fig. 3 — Surface morphology of (a) NFC, (b) plain PLA, (c) PLPF2 and (d) PLPF5

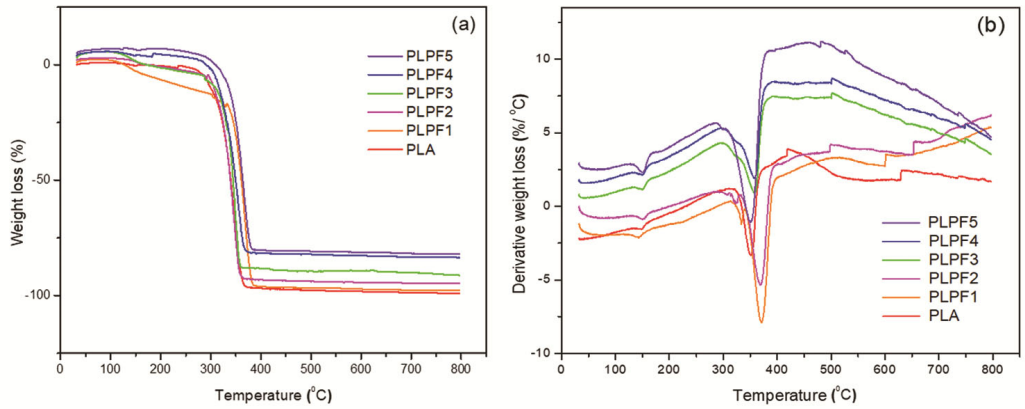

Fig. 4 — (a) TGA and (b) differential thermogravimetric DTA curves of plain PLA and PLA nanocomposites

5 wt% of NFC content has non-uniform distribution of NFC within the polymer matrix as shown in Fig. 3(d). This results in formation of minor gaps, and bright, spherical clusters of NFC on the surface. This clustering is likely due to the formation of strong hydrogen bonds between the cellulose fibers, causing them to self-associate instead of dispersing uniformly. This can lead to phase separation, which may disrupt the uniformity and create weak spots in the nanocomposite films [29,30].

Thermal endurance assessment

The thermal analysis of PLA nanocomposites reveals important insights into their degradation behaviour. The TGA and DTA curves of plain PLA and PLA nanocomposites are shown in Fig. 4(a) and (b), respectively. The corresponding thermal degradation parameters are summarized in Table 2. The thermograms reveal three distinct decomposition phases. The first phase, up to 150°C, involves the

release of absorbed moisture. This is followed by the breakdown of glycosidic bonds of cellulose chains between 200°C and 300°C, during which the nanocomposites undergo around 18% weight loss. In the third phase, from 300°C to 360 °C, the polymer chain backbones undergo fragmentation, with all samples experiencing close to 50% weight loss[31]. This phase marks the main thermal decomposition of PLA nanocomposites occurs at higher temperature than plain PLA, whose main decomposition ends at 351°C. This indicates that addition of NFC enhances the thermal endurance of PLA, implying beneficial impact of NFC reinforcement on the material's thermal resistance. The weight loss percentages observed for the PLA nanocomposites further support this trend, as reduced weight loss correlates with greater thermal resistance. The weight loss percentage of PLPF1 is 96.74%, PLPF2 is 96.23%, PLPF3 is 94.70%, PLPF4 is 92.74 and PLPF5 is 88.25%. This weight loss reduction indicates improved thermal properties and greater resilience to thermal decomposition in the nanocomposites compared to plain PLA, which has a total weight loss of 94.34%. The DTA curves further confirms shift in decomposition temperature to higher ranges (351°C–378°C) for the nanocomposites reflecting better thermal resistance. The maximum decomposition temperature rises by 27°C with increasing NFC content, underscoring the reinforcing effect of NFC on the thermal stability of PLA [32,33].

Table 2 — TGA data for plain PLA and PLA nanocomposites

Sample	T_{onset} (°C)	$T_{50\%}$ (°C)	T_{max} (°C)	Weight loss (%)
PLA	146.94	343.92	351.25	1.676
PLPF1	148.02	347.18	355.84	1.699
PLPF2	156.25	351.25	359.23	2.184
PLPF3	158.48	354.12	366.35	3.251
PLPF4	154.17	359.82	372.84	3.825
PLPF5	150.23	365.25	378.23	4.230

Mechanical performance assessment

Tensile testing was conducted to assess the effect of NFC on the mechanical properties of PLA. The tensile strength, Young's modulus, and elongation at break (EB) of the PLA nanocomposites and plain PLA are shown in Fig. 5. The plain PLA exhibits a tensile strength of 12.24 MPa, which increases to 20.67 MPa with the addition of 5 wt% NFC, showing a 68.8% improvement. This enhancement is attributed to the reinforcing capability of NFC, whose high surface area promotes seamless load transfer within the PLA matrix, thereby strengthening its ability to bear applied stresses. In the same way, the tensile modulus of the nanocomposite films increased by 89.4%, reaching 864.32 MPa at 5 wt% NFC concentration. This increase is due to the rigid and high crystalline nature of NFC, which impedes the polymer chain motion, resulting in a stiffer, more rigid composite[34]. However, the elongation at break decreases progressively by 38.9% with increasing NFC content, suggesting a transition towards more brittle behaviour. This decrease in flexibility is a consequence of the stiffening effect of NFC, which limits the capacity of nanocomposite to bend and expand under stress, thus making it more brittle. These findings reveal that although NFC act as highly efficient reinforcement agent, boosting the tensile strength and modulus of PLA, higher NFC concentration simultaneously make the material more brittle and less flexible[35].

Antibacterial effectiveness

The antibacterial effect was tested against two Gram-positive bacteria (*Bacillus subtilis* and *Staphylococcus aureus*) and two gram-negative bacteria (*Escherichia coli* and *Pseudomonas aeruginosa*). The zone of inhibition of plain PLA and PLA nanocomposites is shown in Fig. 6. The antibacterial performance of PLA nanocomposites is significantly enhanced with the inclusion of NFC, especially in PLPF5, which showed the highest inhibition zones against all bacterial strains. The sample PLPF5 exhibited inhibition zones of

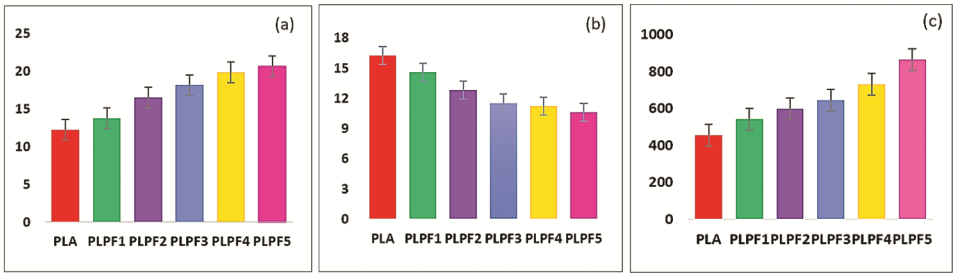

Fig. 5 — Mechanical properties of plain PLA and PLA nanocomposites: (a) tensile strength, (b) elongation at break and (c) Young's modulus

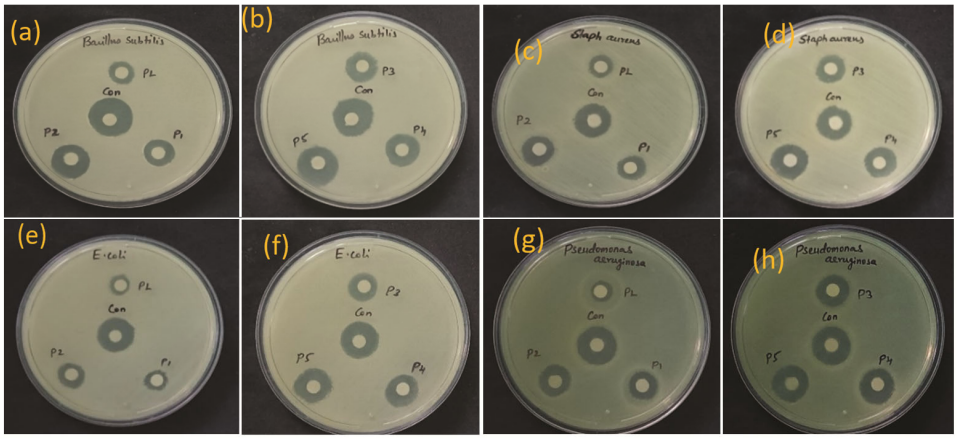

Fig. 6 — Antibacterial activity of plain PLA and 1wt% to 5wt% NFC containing PLA nanocomposites against: (a) and (b) *Bacillus subtilis,* (c) and (d) *Staphylococcus aureus,* (e) and (f) *Escherichia coli*, (g) and (h) *Pseudomonas aeruginosa*

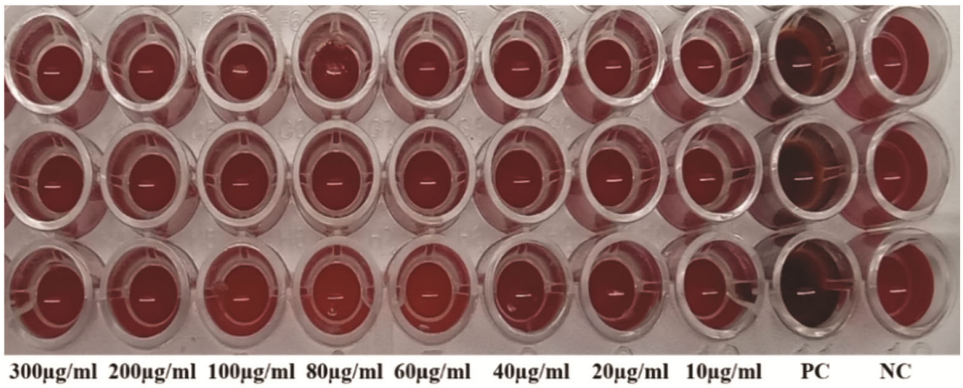

Fig. 7 — Hemolytic response of PLPF3 at different concentrations (300 µg/mL, 200 µg/mL, 100 µg/mL, 80 µg/mL, 60 µg/mL, 40 µg/mL, 20 µg/mL and 10 µg/mL), the positive control (PC) shows complete hemolysis, while the negative control (NC) indicates non-hemolysis

Table 3 — Hemolysis effect of PLPF3 on human erythrocytes

Sl. No.	Concentration of PLPF3 (µg/mL)	Optical density at 545nm	Hemolysis (%)
1.	Positive control	2.333 ± 0.0412	100
2.	Negative control	1.193 ± 0.0136	0
3.	10	1.054 ± 0.0236	0
4.	20	1.034 ± 0.0188	0
5.	40	1.072 ± 0.0212	0
6.	60	1.088 ± 0.0065	0
7.	80	1.122 ± 0.0219	0
8.	100	1.148 ± 0.0578	0.273 ± 0.016
9.	200	1.126 ± 0.0182	1.321 ± 0.023
10.	300	1.306 ± 0.0302	4.542 ± 1.342

16.6 mm against *B. subtilis*, 16.5 mm against *S. aureus*, 16.2 mm against *E. coli*, and 16.2 mm against *P. aeruginosa*. This performance was comparable to the antibiotic control Amikacin, which showed inhibition zones of 17 mm, 16 mm, 17 mm, and 18 mm for the same bacteria. While, plain PLA showed much lower antibacterial performance, with inhibition zones of 12 mm, 10.6 mm, 9.5 mm, and 9 mm, respectively. This improvement can be ascribed to the high concentration and dispersion of NFC, which increased the surface area and provided more interaction sites for bacterial cells, enabling better disruption of cell walls and suppressing bacterial growth [36].

Hemolytic activity of PLPF3 on human erythrocytes

The hemolysis study of the PLA nanocomposite film (PLPF3) demonstrates exceptional hemo compatibility according to ISO 10993-4 standards, which categorize materials based on their hemolysis percentage: less than 2% is considered non-hemolytic, 2-5% indicates mild hemolysis, and above 5% suggests hemolytic activity [37,38]. The results of the hemolysis assay for PLPF3 are provided in Table 3. The interaction of PLPF3 with red blood cells, reflecting its hemolytic activity, is illustrated in Fig. 7. As shown in the table, at concentrations of 10 µg/mL,

20 µg/mL, 40 µg/mL, 60 µg/mL, 80 µg/mL, 100 µg/mL, and 200 µg/mL, non hemolysis was observed, with optical density values close to the negative control (OD: 1.193), indicating no adverse effects on red blood cells. At 300 µg/mL, hemolysis increased to 4.54%, which falls within the mild hemolysis range according to the ISO classification. These results confirm that PLPF3 is a biocompatible material with minimal red blood cell damage, making it suitable for blood-contacting biomedical applications.

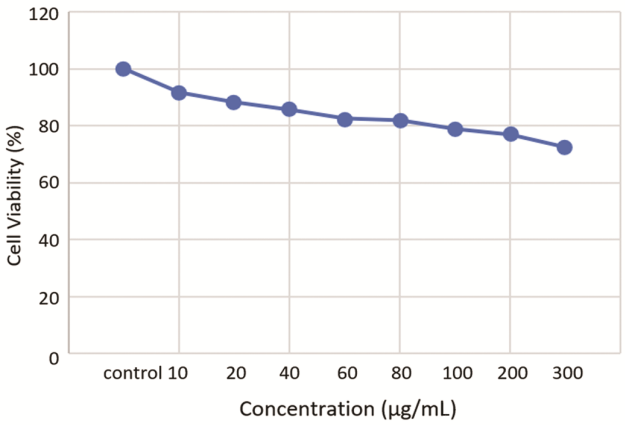

Fig. 8 — Cell viability percentage of peripheral blood mononuclear cells treated with PLPF3

In vitro cytotoxicity evaluation of PLPF3

The MTT assay was performed on Peripheral Blood Mononuclear Cells (PBMCs) in direct contact with the PLPF3 nanocomposite film to assess its cytotoxicity. According to ISO 10993-5 standards the materials with cell viability above 70% are considered non-cytotoxic [39,40]. Fig. 8 presents the graphical representation of the overall percentage of cell viability. Fig. 9(a)–9(d) show microscopic images of cell viability for the control and PLPF3 treated samples at varying concentrations. The graph shows that at a concentration of 300 µg/mL, cell viability

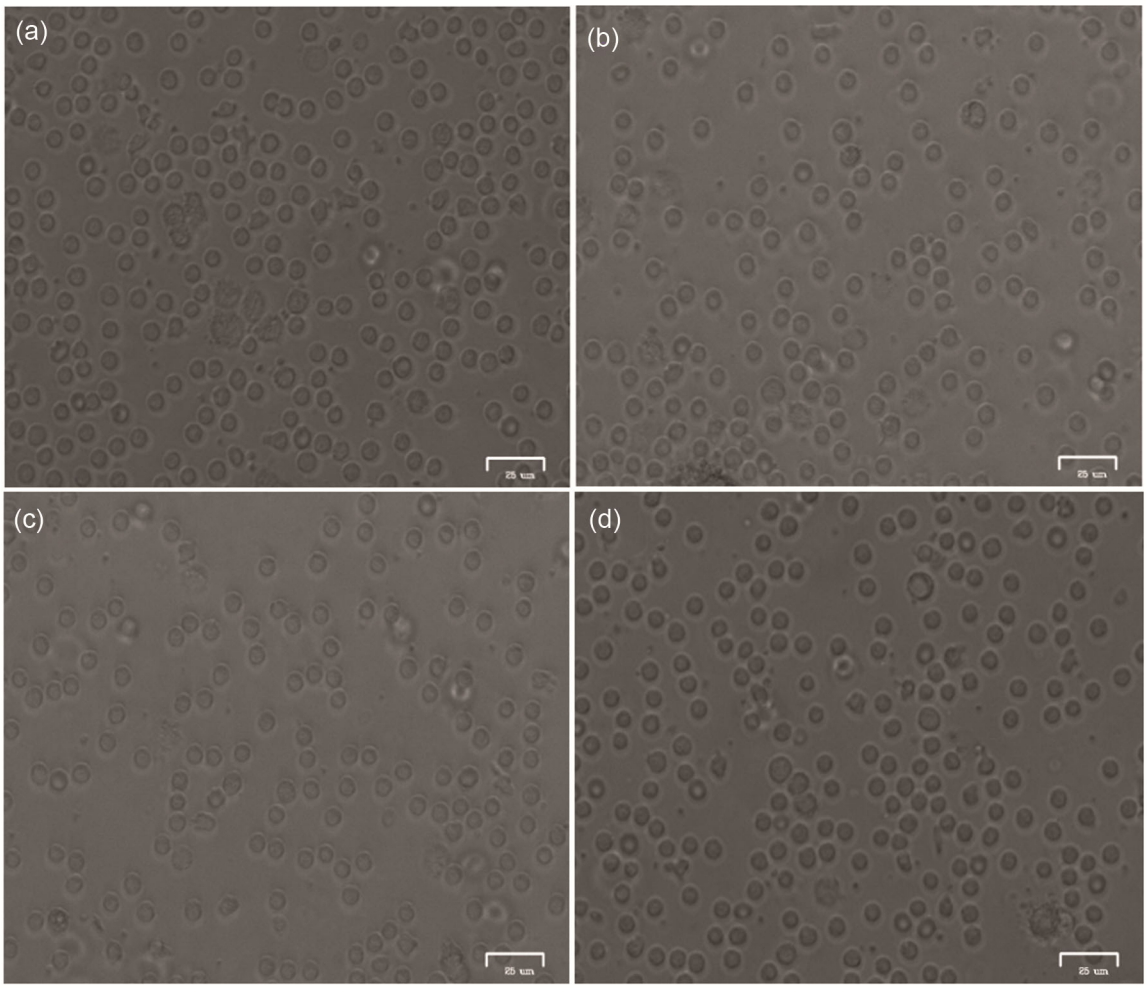

Fig. 9 — Cell viability of PLPF3 at varying Concentrations: (a) control, (b) 10 µg/mL, (c) 80 µg/mL and (d) 200 µg/mL

was 72.37%, indicating mild cytotoxicity. As the concentration decreased, cell viability increased. At 200 µg/mL, cell viability rise to 76.99%, followed by 78.87% at 100 µg/mL, 81.75% at 80 µg/mL, and 82.51% at 60 µg/mL. Further reductions in concentration to 40 µg/mL, 20 µg/mL, and 10 µg/mL resulted in even greater cell viabilities of 85.52%, 88.26%, and 91.48%, respectively. The higher cell viability indicates improved cell growth and reduced cytotoxic effects. Therefore, decreasing the concentration of PLPF3 increased cell viability, indicating reduced toxicity and better cell proliferation, making the nanocomposite suitable for biomedical applications[39,40].

Conclusion

The incorporation of Palmyra nanofibrillated cellulose (NFC) into polylactic acid (PLA) significantly enhances the thermal, mechanical and biocompatible properties of the nanocomposites. FTIR analysis reveals a peak at 1245 cm^{-1} corresponding to the C–O stretching group of cellulose, confirming the incorporation of NFC into the PLA matrix. SEM analysis shows that the fibrillar structure of NFC increases the surface area for polymer chain interactions leading to consistently dispersed NFC at lower filler content without clumping. TGA and DTA analyses indicates rise in decomposition temperature from 351°C to 388°C with higher NFC loadings. XRD analysis reveals enhanced crystallinity of 84.7% with increasing NFC content which aids the improved mechanical performance of the nanocomposites. Tensile testing shows marked rise in tensile strength (20.67 MPa) and tensile modulus (864.32 MPa) as the NFC content increases up to 5 wt%, while elongation at break sharply drops to 38.9% due to the natural stiffness of NFC. The antibacterial activity of the PLA nanocomposites is increased due to the increasing content of NFC which serves as strong antibacterial agent and offering better inhibition of bacterial colonies compared to plain PLA. Hemolysis and MTT assay demonstrated excellent biocompatibility of 3 wt% NFC loading, with minimal red blood cell impairment and high cell viability. These enhancements make the nanocomposites ideal for biomedical applications, including medical devices, wound dressings, and drug delivery systems, providing sustainable and reliable material solution.

Acknowledgments

The authors would like to express their sincere gratitude to VOC College, Tuticorin, VIT Institute of Technology, Vellore, Annamalai University, Chennai, ManonmaniamSundaranar University, Tirunelveli, Sree Chitra Tirunal Institute for Medical Sciences and Technology, Trivandrum and Trichy research institute of biotechnology private limited, Trichy for their invaluable support in sample analysis.

Conflicts of Interest

The authors affirm that they have no competing interests.

References

1 Ranakoti L, Gangil B, Mishra S K, Singh T, Sharma S, Ilyas R A & El-Khatib S, Critical review on polylactic acid: Properties, structure, processing, biocomposites, and nanocomposites, *Mater*, 15 (2022) 4312.

2 Taib N A A B, Rahman M R, Huda D, Kuok K K, Hamdan S, Bakri M K B, Julaihi M R M B & Khan A, Review on poly lactic acid (PLA) as a biodegradable polymer, *Polym Bullet* 80 (2023) 1179.

3 Bikiaris N D, Koumentakou I, Samiotaki C, Meimaroglou D, Varytimidou D, Karatza A, Kalantzis Z, Roussou M, Bikiaris R D & Papageorgiou G Z, Recent advances in the investigation of poly(lactic acid) (PLA) nanocomposites: Incorporation of various nanofillers and their properties and applications, *Polymer*, 15 (2023) 1196.

4 Auras R, Harte B & Selke S, An overview of polylactides as packaging materials, *Macromol Biosci*, 4 (2004) 835.

5 Drumright R E, Gruber P R & Henton D E, Polylactic acid technology, *Adv Mater*, 12 (2000) 1841.

6 Lunt J, Large-scale production, properties and commercial applications of polylactic acid polymers, *Polym Degrad Stab*, 59 (1998) 145.

7 Gupta A P & Kumar V, New emerging trends in synthetic biodegradable polymers-Polylactide: A critique, *Eur Polym J*, 43 (2007) 4053.

8 Millet H, Vangheluwe P, Block C, Sevenster A, Garcia L & Antonopoulos R, The nature of plastics and their societal usage, In R M Harrison & R E Hester, (Eds.), Plastics and the Environment, *Royal Soc Chem*, 1 (2018) 1.

9 Garlotta D A, A literature review of poly(lactic acid), *J Polym Environ*, 9 (2001) 63.

10 Ray S S & Bousmina M *J,* Biodegradable polymers and their layered silicate nanocomposites: In greening the 21st century materials world, *Polym Environ*, 13 (2005) 297.

11 Auras R A, Lim L T, Selke S E M & Tsuji H, Polylactic acid: Synthesis, properties and applications, *Monom Polym Compos Renew Resour*, 1 (2008) 433.

12 Khouri N G, Bahú, J O, Blanco-Llamero, C, Severino P, Concha, V O C & Souto E B, Polylactic acid (PLA): Properties, synthesis, and biomedical applications-A review of the literature, *J Mol Struct*, 1309 (2024) 138243.

13 Fortunati E, Luzi F, Yang W, Kenny J M, Torre L & Puglia D, Bio-based nanocomposites in food packaging, *Nanomater*

Food Packag: Mater Process Technol Saf Issues Micro Nano Technol, 1 (2016) 71.

14 Miao C & Hamad W Y, Cellulose reinforced polymer composites and nanocomposites: A critical review, *Cellulose*, 20 (2013) 2221.

15 Tang J, Sisler J, Grishkewich N & Tam K C, Functionalization of cellulose nanocrystals for advanced applications, review: Current international research into cellulose nanofibres and nanocomposites, *J Colloid Interf Sci*, 49 (2017) 397.

16 Eichhorn S J, Dufresne A, Aranguren M, Marcovich N E, Capadona J R, Rowan S J, Weder C, Thielemans W, Roman M, Renneckar S, Gindl W, Veigel S, Keckes J, Yano H, Abe K, Nogi M, Nakagaito A N, Mangalam A, Simonsen J, Benight A S, Bismarck A, Berglund L A & Peijs T, Review: Current international research into cellulose nanofibres and nanocomposites, *J Mater Sci*, 45 (2010) 1.

17 Ansari M M, Heo Y, Do K, Ghosh M & Son Y O, Nanocellulose derived from agricultural biowaste by-products-Sustainable synthesis, biocompatibility, biomedical applications, and future perspectives: A review, *Carbohydr Polym Technol Appl*, 8 (2024) 100529.

18 Noremylia, M B, Hassan M Z & Ismail Z, Recent advancement in isolation, processing, characterization and applications of emerging nanocellulose: A review, *Int J Biol Macromol*, 206 (2022) 954.

19 Aman A, Rajan R & Sinha S, The palmyrah palm (Borassus flabellifer L.): Overview of biology, uses, and cultivation, *Biomol Rep*, **(**2022)**.**

20 Behera S, Phytochemical constituents and nutritional potential of palmyra palm: A review, *Academia Edu*, 42 (2023) 211.

21 Rao S, Madhushree M & Bhat K S, Characteristics of surface modified sugarcane bagasse cellulose: Application of esterification and oxidation reactions, *Sci Rep*, 14 (2024) 24136.

22 Rahimi K S M, Brown R J, Tsuzuki T & Rainey T J, Comparison of cellulose nanocrystals and cellulose nanofibres extracted from bagasse using acid and ball milling methods, *Adv Nat Sci Nanosci Nanotechnol*, **7** (2016) 035004.

23 Abdulkhani A, Hosseinzadeh J, Ashori A, Dadashi S & Takzare Z, Preparation and characterization of modified nanofibrillated cellulose reinforced polylactic acid nanocomposite, *Polym Testing*, 35 (2014) 73.

24 Wang L F, Shankar S & Rhim J W, Properties of alginate-based films reinforced with cellulose fibers and cellulose nanowhiskers isolated from mulberry pulp, *Food Hydrocolloids*, 63 (2017) 201.

25 Flauzino-Neto W P, Silvério H A, Dantas N O & Pasquini D, Extraction and characterization of cellulose nanocrystals from agro-industrial residue-Soy hulls, *Ind Crops Prod*, 42 (2013) 480.

26 Dhar P, Bhasney, S M, Kumar A & Katiyar V, Acid functionalized cellulose nanocrystals and its effect on mechanical, thermal, crystallization and surface properties of poly(lactic acid) bionanocomposites films: A comprehensive study, *Polymer*, 101 (2016) 75.

27 Chang C, Hou J, Chang P R & Huang J, Structure and properties of cellulose nanocrystals, Huang J, Dufresne A & Lin N, (Eds.), *J Nanomater*, 42 (2017) 54.

28 Frone A N, Panaitescu D M, Chiulan I, Nicolae C A, Vuluga Z, Vitelaru C & Damian C M, The effect of nanofibrillated cellulose on the crystallinity and nanostructure of poly (lactic acid) composites, *J Mater Sci*, 51 (2016) 9771.

29 Wang Q, Ji C, Sun J, Zhu Q & Liu J, Structure and properties of polylactic acid biocomposite films reinforced with cellulose nanofibrils, *Molecules*, 25 (2020) 3306.

30 Zhang B, Huang C, Zhao H, Wan J, Yin C, Zhang L & Zhao Y, Effects of cellulose nanocrystals and nanofibrillated cellulose on the structure and properties of polyhydroxybutyrate nanocomposites, *Polymer*, 11 (2019) 2063.

31 Ruz-Cruz M A, Herrera-Franco P J, Flores-Johnson E A, Moreno-Chulim M V, Galera-Manzano L M & Valadez-González A, Thermal and mechanical properties of PLA-based multiscale cellulosic biocomposites, *J Mater Res Technol,* 18 (2022) 485.

32 Dhar M P & Katiyar V, Thermal degradation kinetics of polylactic acid/acid fabricated cellulose nanocrystal based bionanocomposites, *Int J Biol Macromol*, 104 (2017) 827.

33 Raisipour-Shirazi A, Ahmadi Z & Garmabi H, Polylactic acid nanocomposites toughened with nanofibrillated cellulose: Microstructure, thermal, and mechanical properties, *Iran Polym J*, 27 (2018) 785.

34 Mokhena T C, Sadiku E R, Mochane, M J, Ray S S, John M J & Mtibe A, Mechanical properties of cellulose nanofibril papers and their bionanocomposites: A review, *Carbohydr Polym*, 273 (2021) 118507.

35 Helbert W, Cavaillé J Y & Dufresne A, Thermoplastic nanocomposites filled with wheat straw cellulose whiskers. Part I: Processing and mechanical behavior, *Polym Compos,* 17 (1996) 604.

36 Rashki S, Shakour N, Yousefi Z, Rezaei M, Homayoonfal M, Khabazian E, Atyabi F, Aslanbeigi F, Lapavandani R S, Mazaheri S, Hamblin M R & Mirzaei H, Cellulose-based nanofibril composite materials as a new approach to fight bacterial infections, *Front Bioeng Biotechnol,* **9** (2021) 1.

37 Liu H Y, Du L, Zhao Y T & Tian W Q, In vitro hemocompatibility and cytotoxicity evaluation of halloysite nanotubes for biomedical application, *J Nanomater,* (2015) 9.

38 Jerlite K J J & Nevaditha N T, Thermal degradation and hemocompatibility of polyurethane cellulose nano-composites, *Int J Health Sci*, 6 (2022) 5613.

39 Singh M, Singh R K, Singh S K, Mahto S K & Misra N, In vitro biocompatibility analysis of functionalized poly(vinyl chloride)/layered double hydroxide nanocomposites, *RSC Adv,* 8 (2018) 40611.

40 Promdontree P, Kheolamai P, Ounkaew A, Narain R & Ummartyotin S, Characterization of cellulose fiber derived from hemp and polyvinyl alcohol-based composite hydrogel as a scaffold material, *Polym*, 15 (2023) 4098.